AGU PUBLICATIONS

Paleoceanography

RESEARCH ARTICLE
10.1002/2013PA002492

Key Points:
- Global preservation-dissolution pattern for planktonic foraminiferal Mg/Ca
- Bottom water calcite-saturation state controls Mg/Ca dissolution
- Mg/Ca dissolution is similar for all foraminiferal species and ocean basins

Supporting Information:
- Readme
- Figures S1–S5 and Tables S1–S3

Correspondence to:
M. Regenberg,
regenberg@gpi.uni-kiel.de

Citation:
Regenberg, M., A. Regenberg, D. Garbe-Schönberg, and D. W. Lea (2014), Global dissolution effects on planktonic foraminiferal Mg/Ca ratios controlled by the calcite-saturation state of bottom waters, *Paleoceanography*, *29*, 127–142, doi:10.1002/2013PA002492.

Received 9 APR 2013
Accepted 3 JAN 2014
Accepted article online 8 JAN 2014
Published online 1 MAR 2014

Global dissolution effects on planktonic foraminiferal Mg/Ca ratios controlled by the calcite-saturation state of bottom waters

Marcus Regenberg[1], Anke Regenberg[1], Dieter Garbe-Schönberg[1], and David W. Lea[2]

[1]Institute of Geosciences, Christian-Albrechts-Universitöt, Kiel, Germany, [2]Department of Earth Science and Marine Science Institute, University of California, Santa Barbara, California, USA

Abstract Mg/Ca ratios of planktonic foraminiferal tests are important tools for reconstructing past ocean temperatures at different levels of the upper water column. Yet numerous studies suggest a significant influence of calcite dissolution on Mg/Ca ratios lowering their initial signal recorded within a planktonic foraminiferal habitat. To determine the effect of dissolution, this study presents Mg/Ca ratios of eight planktonic foraminiferal species from the South China Sea sediment surface. Continuously decreasing with increasing water depth, the Mg/Ca ratios also decrease with calcite-saturation states close to and below saturation (bottom water $\Delta[CO_3^{2-}]$ <30 μmol kg^{-1}) but are stable in well calcite-supersaturated bottom waters (>40 μmol kg^{-1}). This preservation pattern compares well with examples of Mg/Ca dissolution from the tropical Atlantic Ocean and is independent of the foraminiferal species. Merging a global data set by separate normalization of 79 Mg/Ca data sets from the Pacific, Atlantic, and Indian Oceans, which removes thermal differences between the ocean regions and foraminiferal species, enabled us to quantify a global decrease in planktonic foraminiferal Mg/Ca ratios of 0.054 ±0.019 μmol mol^{-1} per μmol kg^{-1} below a critical threshold for dissolution of 21.3 ±6.6 μmol kg^{-1}. The absolute decline in Mg/Ca ratios, which is similar for all species, affects temperature estimates from (sub-)thermocline species more strongly than those from shallow dwellers. The water depth of this critical threshold in the global oceans shoals from >3.5 km in the North Atlantic to <0.5 km in the North Pacific based on calculations of the global calcite-saturation state from 6321 hydrographic stations. Above this critical threshold Mg/Ca ratios are well preserved, and paleotemperature estimates are broadly unaffected by dissolution.

1. Introduction

Mg/Ca ratios of planktonic foraminiferal tests precipitated at distinct water depth levels in shallow, intermediate, and deep habitats [e.g., *Fairbanks et al.*, 1982; *Farmer et al.*, 2007; *Steph et al.*, 2009] have been effectively used to assess past ocean temperatures. Variations in Mg/Ca-derived paleotemperature estimates are appropriate for inferring changes in periodic phenomena [e.g., *Koutavas et al.*, 2002; *Schmidt et al.*, 2006] and long-term variability of climate [e.g., *Holbourn et al.*, 2010; *Lea et al.*, 2000], and for reconstructions of ocean stratification [e.g., *Regenberg et al.*, 2009; *Xu et al.*, 2010] and circulation patterns [e.g., *Pahnke et al.*, 2003; *Ziegler et al.*, 2008]. The use of foraminiferal Mg/Ca ratios as a paleotemperature proxy is based on the exponentially enhanced substitution of Mg^{2+} for Ca^{2+} (reported as Mg/Ca ratio) during test precipitation at higher ambient seawater temperatures [e.g., *Anand et al.*, 2003; *Elderfield and Ganssen*, 2000; *Lea et al.*, 1999; *Regenberg et al.*, 2009]. Calculated paleotemperatures from initial Mg/Ca ratios, which are recorded during test precipitation, are typically associated with an uncertainty of 1.0–1.4°C [*Anand et al.*, 2003; *Dekens et al.*, 2002; *Regenberg et al.*, 2009]. This uncertainty and consequently the success of Mg/Ca paleothermometry can be corrupted by diagenetic alterations of the initial Mg/Ca signature after foraminiferal tests have settled on the seafloor [e.g., *Barker et al.*, 2003; *Lorens et al.*, 1977; *Regenberg et al.*, 2007].

A decrease in Mg/Ca ratios accompanies partial dissolution of foraminiferal calcite [*Brown and Elderfield*, 1996; *Fehrenbacher et al.*, 2006]. The Mg/Ca decrease is coupled with test-weight loss even at shallow seafloors located above the calcite-saturation horizon [*de Villiers*, 2005; *Rosenthal and Lohmann*, 2002], where overlying bottom waters are supersaturated with respect to pure calcite ($\Delta[CO_3^{2-}]$>0 μmol kg^{-1}, Ω >1). Progressive calcite dissolution in deeper and less calcite-supersaturated to undersaturated ($\Delta[CO_3^{2-}]$ <0 mol kg^{-1}, Ω <1) bottom waters causes Mg/Ca ratios to decrease [Dekens *et al.*, 2002; Johnstone *et al.*, 2011; Regenberg *et al.*, 2006], fragmentation of foraminiferal tests [*Conan et al.*, 2002; *Mekik and*

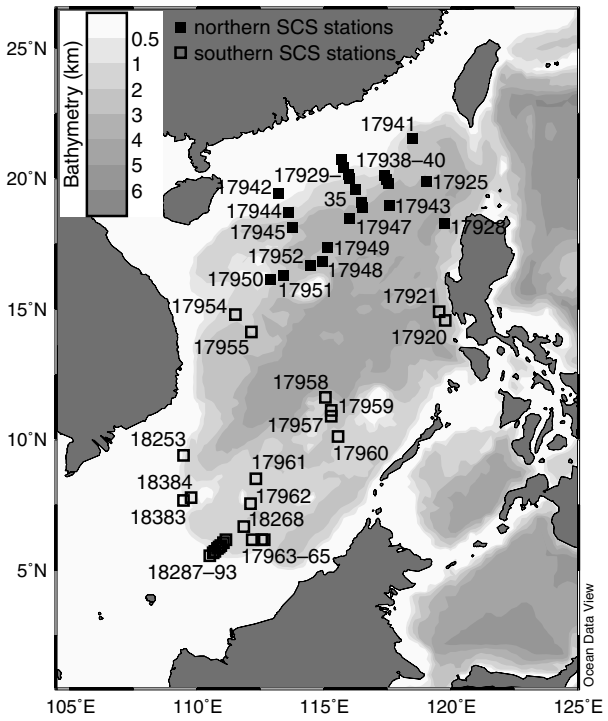

Figure 1. Bathymetric chart of the South China Sea showing the locations of the northern (filled squares) and southern SCS (open squares) sediment-surface samples used in this study [*Sarnthein et al.*, 1994; *Stattegger et al.*, 1997; *Wiesner et al.*, 1999].

François, 2006], and their final absence from sediments at the snowline of the calcite-compensation depth (100% $CaCO_3$ dissolution) with $\Delta[CO_3^{2-}]$ of about −30 μmol kg^{-1} at the bottom water-sediment interface [*Archer*, 1996]. Previous findings of dissolution effects on Mg/Ca ratios depending on the foraminiferal species and the ocean basin [e.g., *Brown and Elderfield*, 1996; *Dekens et al.*, 2002; *Johnstone et al.*, 2011; *Regenberg et al.*, 2006] are based on data sets limited in sample and species numbers. It is thus still disputable whether or not the decrease in Mg/Ca ratios is dependent on the foraminiferal species and uniform at different seawater $\Delta[CO_3^{2-}]$, and from which $\Delta[CO_3^{2-}]$ value and water depth Mg/Ca ratios are subject to dissolution.

Mg/Ca ratios from equatorial Pacific sediment-surface samples were interpreted to continuously decrease with increasing water depth of planktonic foraminiferal test deposition [*Lea et al.*, 2000]. In contrast, Caribbean Mg/Ca ratios only decrease below 2.5 km water depth, while tests with stable Mg/Ca signals from shallower samples were deposited well above the calcite-saturation horizon [*Regenberg et al.*, 2006]. To validate these supposedly contradictory dissolution effects on Mg/Ca ratios and their dependence on water depth or $\Delta[CO_3^{2-}]$, we performed 516 Mg/Ca measurements of planktonic foraminiferal tests from 48 South China Sea (SCS) sediment-surface samples (Figure 1) [*Sarnthein et al.*, 1994; *Stattegger et al.*, 1997; *Wiesner et al.*, 1999]. Since the SCS is the most undersaturated marginal sea with respect to calcite in the tropics, the foraminiferal tests were exposed to bottom waters with low $\Delta[CO_3^{2-}]$ even at a shallow seafloor. Although the SCS Mg/Ca data sets of eight planktonic foraminiferal species seem to show continuous decreases with increasing water depth from the shallowest to deepest samples (329–3795 m), we demonstrate here that Mg/Ca ratios are exempt from dissolution effects in sediments above ≈400 m water depth, where $\Delta[CO_3^{2-}]$ of bottom waters are >40 μmol kg^{-1}. Only at lower $\Delta[CO_3^{2-}]$ in deeper bottom waters Mg/Ca ratios show a decreasing trend. Combination with 13 studies composed of 63 sediment-surface multispecies Mg/Ca data sets reveals a global control of $\Delta[CO_3^{2-}]$ of bottom waters on the preservation of planktonic foraminiferal Mg/Ca ratios valid for all ocean basins and planktonic foraminiferal species.

2. Upper Ocean Temperatures in the South China Sea

Prominent temperature variation in the SCS is restricted to the mixed layer [*Zhou and Gao*, 2003], where salinity is also quite variable due to basin-wide precipitation, river runoff from the surrounding landmasses,

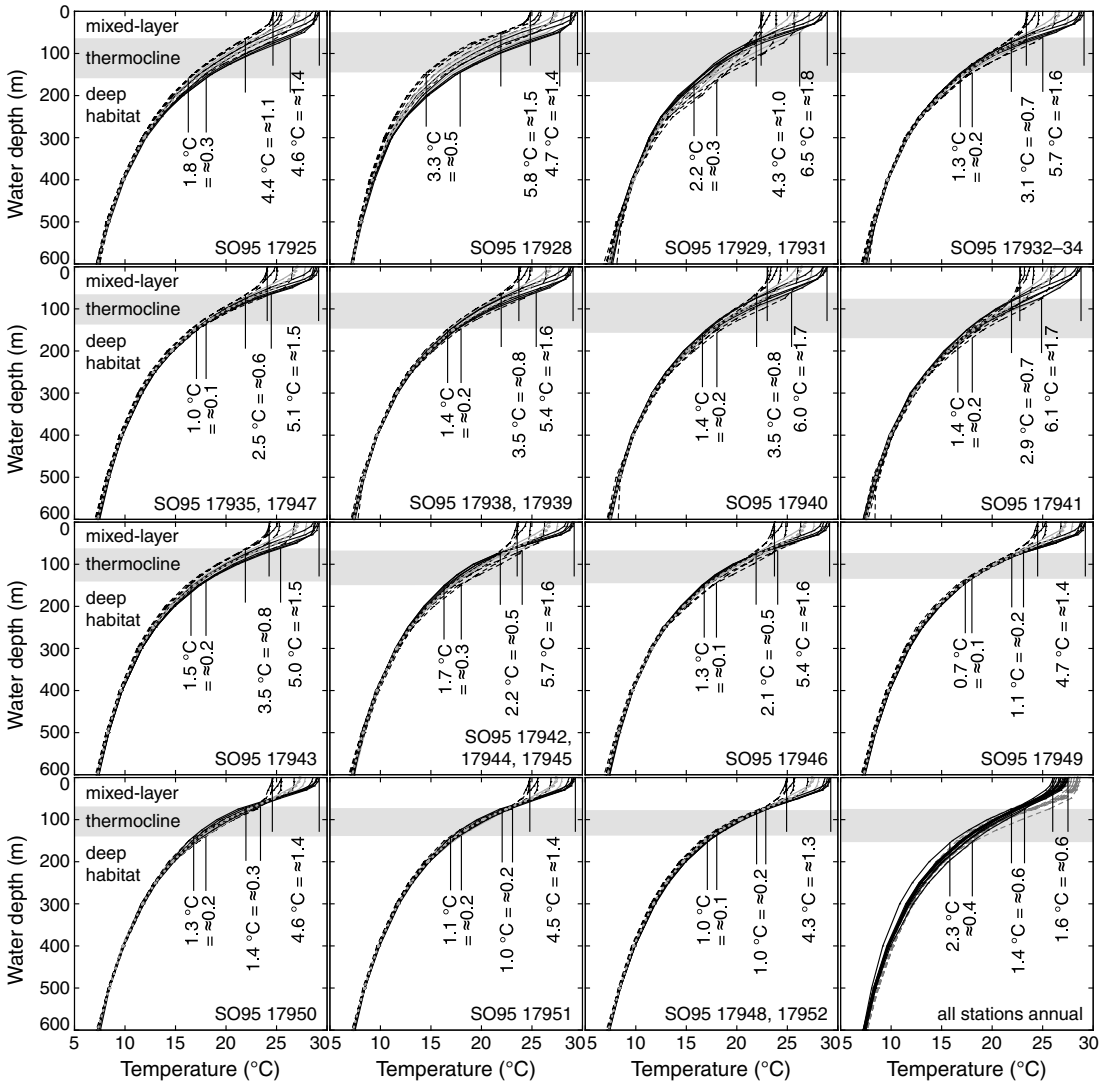

Figure 2. Temperature profiles at World Ocean Atlas 2001 grid points [*NODC*, 2001] nearest to the indicated northern SCS stations: annual mean (stippled lines), May–September (black solid lines), November–March (dashed lines), October and April (grey solid lines). Lowermost right panel compares the annual mean temperature profiles from the northern SCS (solid lines) with those from the southern SCS (stippled lines). Temperature variations given for the sea surface, the top and the base of the thermocline (shaded area) are converted into Mg/Ca in mmol mol^{-1} applying standard calibrations indicating a 9% increase in Mg/Ca ratios per °C [e.g., *Lea et al.*, 2000; *Dekens et al.*, 2002; *Anand et al.*, 2003].

and advection of deeper water masses [*Wang and Li*, 2009; *Wang and Wang*, 2006]. During the weaker and wetter southwest monsoon (May to September), surface water temperatures of the warm pool peak at >29°C. Contrarily, lowest temperatures in February of ≈ 24°C are attained after a rapid drop during the stronger and drier northeast monsoon (November to March) [*Chen et al.*, 2003; *Chu and Guihua*, 2003; *Haijun et al.*, 1999; *Wang and Wang*, 2006], elevated by up to 2°C during El Niño events 1997–1998 and 2002–2003 [*Tseng et al.*, 2009a, 2009b]. Seasonal thermal variability, however, is higher in the more saline northern SCS (≈6°C) than in the southern SCS (≈3°C), which belongs to the West Pacific Warm Pool [*Wang and Li*, 2009]. Such differences between the northern and southern SCS are due to a thermohaline front located between the South Vietnam coast at ≈15°N in the west and Luzon Island at ≈19°N in the east [*Chu and Guihua*, 2003].

Between the stations of this study, annual temperature variation in the mixed layer is maximal ≈ 2.6°C with lower temperatures in the northern SCS than in the southern SCS (Figures 2 and 3). In the southern SCS, annual mixed-layer temperatures vary by ≈ 0.8°C, in the northern SCS by ≈ 1.5°C [*National Oceanographic and Data Center* (*NODC*), 2001]. On average, annual mixed-layer temperatures at the southern SCS stations are higher by ≈1.5°C (0.2–2.6°C) than at the northern SCS stations. Annual temperature variation at

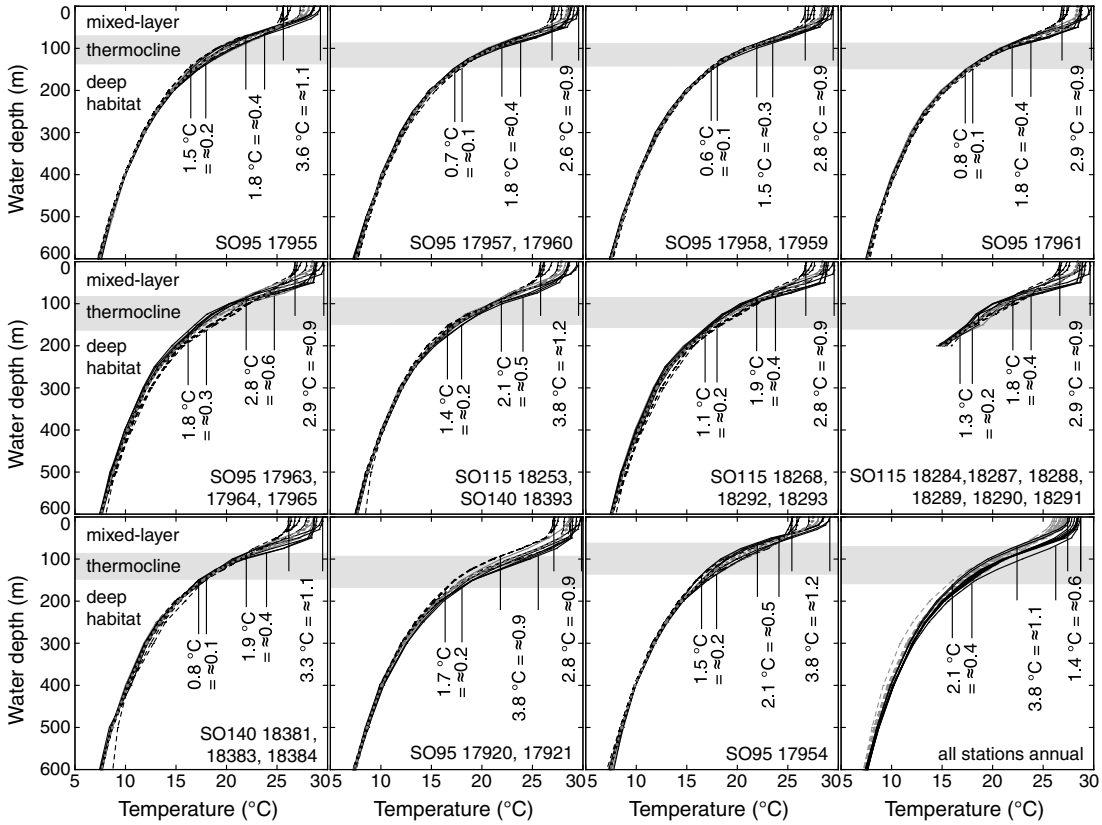

Figure 3. Temperature profiles at World Ocean Atlas 2001 grid points [*NODC*, 2001] nearest to the indicated southern SCS stations. Details as in Figure 2.

the top of the SCS seasonal thermocline, defined as interval between the 18 and 22°C isotherms, is ≈1.4°C between the northern stations and ≈1.9°C between the southern stations. On average, annual thermocline temperatures at the southern SCS stations are higher by ≈2.2°C (0.5–3.9°C) than at the northern SCS stations. At the top of the SCS permanent thermocline (<18°C isotherm), temperature varies by ≈2.1°C at the northern stations enveloping the southern variation of ≈1.0°C.

Monthly temperature variation at the northern stations is on average ≈5.3°C (4.3–6.5°C) at the surface, ≈2.9°C (1.0–5.8°C) at the top of the seasonal thermocline, and ≈1.5°C (0.7–3.3°C) at the top of the permanent thermocline (Figure 2). At the southern stations, average monthly temperature variation is ≈3.0°C (2.6–3.8°C) at the surface, ≈2.1°C (1.5–3.8°C) at the top of the seasonal thermocline, and ≈1.2°C (0.6–1.8°C) at the top of the permanent thermocline (Figure 3).

3. Material and Methods

The SCS sediment-surface samples (0–1 cm; Figure 1) were recovered during R/V *Sonne* cruise SO95 from spade box cores, SO115 and SO140 from giant box cores [*Sarnthein et al.*, 1994; *Stattegger et al.*, 1997; *Wiesner et al.*, 1999] with generally high sedimentation rates (>5 cm kyr^{-1}), stained benthic foraminifera, and late Holocene ages [cf., *Regenberg et al.*, 2010]. For this study, three shallow and mixed-layer dwelling foraminiferal species (*Globigerinoides ruber* white sensu stricto, *Globigerinoides sacculifer* without sac-like final chamber, *Globorotalia cultrata*), three intermediate and thermocline dwellers (*Pulleniatina obliquiloculata*, *Neogloboquadrina dutertrei*, *Globorotalia menardii*), and two deep and subthermocline dwellers (*Globorotalia scitula*, *Globorotalia truncatulinoides* dextral (mixing poorly and heavily crusted specimens)) were selected.

In total, our 516 Mg/Ca ratios can be divided into three groups of data sets, each containing results for one foraminiferal species, following different cleaning protocols and analytical setups (Table 1). Mg/Ca measurement of 351 samples from 44 stations (Group I and II) was run on the Spectro CirosCCD inductively coupled plasma (ICP) optical emission spectroscopy (OES) at IfG Kiel (Table 1; analytical error for Mg/Ca ratios ≈0.1%,

Table 1. Summary of Grouped Data Sets (= Foraminiferal Species) Presented in This Study

	Number of		Methodology		Setup	
Group	Samples	Data Sets	Size Fraction	Cleaning	Device	Standardization
I	313	8	355–400 μm	Excluded reductive step	ICP OES, Kiel	ECRM 752-1
II	38	6	355–400 μm	Included reductive step	ICP OES, Kiel	ECRM 752-1
III	165	3	300–350 μm	Included reductive step	ICP MS, Santa Barbara	In-house standard

relative standard deviation). For control, the certified reference material ECRM 752-1 (limestone) with an expected Mg/Ca ratio of 3.9 mmol mol^{-1} [*Greaves et al.*, 2008] was run as standard and showed an average Mg/Ca ratio of 3.89 ±0.05 mmol mol^{-1} (n =150) during a period of 11 months. Samples analyzed at University of California Santa Barbara (UCSB) in 2002 include 165 Mg/Ca measurements from 30 stations (Group III, including 23 measurements from four stations not included in Group I and II (Table 1)). These samples were analyzed on a Thermo Finnigan Element2 sector ICP mass spectrometer (MS). Analytical reproducibility was estimated at 1% (1σ). Standardization was based on in-house standards in use at UCSB since the late 1990s. In addition to Mg/Ca, Fe, Al, Mn, and U were measured to assess diagenetic coatings and contaminants [*Lea et al.*, 2005].

Ten to 52 monospecific tests were crushed and homogenized. Samples of Group I were subsequently cleaned with methanol (clay removal), hydrogen peroxide (removal of organic matter), and repeated treatments with ultrapure water before a weak acid leach (removal of high-Mg calcite) and final dissolution [*Barker et al.*, 2003; *Martin and Lea*, 2002]. Samples of Group II were cleaned with an additional hydrazine step (removal of Mn-Fe-(hydr-)oxide) after the methanol step. Samples of Group III were prepared using the full reductive cleaning [*Lea et al.*, 2000; *Martin and Lea*, 2002]. Size fractions in Group I and II were subsequently extended to a maximum of 250–450 μm in ≈ 30% of the samples because of too few material. Group I data sets are extended by 4 Mg/Ca ratios for *G. ruber* [*Steinke et al.*, 2005] and 71 Mg/Ca ratios for *G. cultrata* and *G. menardii* [*Regenberg et al.*, 2010], which are from similar size fractions and followed the same cleaning protocol and analytical setup. On the basis of 38 samples split into halves after crushing, we found low respective mean Fe/Ca and Mn/Ca ratios of 0.06 ±0.05 mmol mol^{-1} and 0.11 ±0.12 mmol mol^{-1} for non-reductively cleaned samples of Group I, and 0.05 ±0.06 mmol mol^{-1} and 0.04 ±0.04 mmol mol^{-1} for hydrazine-cleaned aliquots of Group II indicating weak influence of Mn-Fe-(hydr-)oxide coatings on SCS foraminiferal tests (supporting information Figure S1). Confirming previous studies [e.g., *Bian and Martin*, 2010], our 38 Mg/Ca ratios of hydrazine-cleaned samples of Group II were significantly lower than their non-reductively cleaned aliquots of Group I by ≈ 3% (t test value 0.6 on a 95% confidence interval; supporting information Figure S2). High-sensitivity ICPMS measurements of Fe revealed that some shallow samples contained very high levels of Fe/Ca ratios, which likely relate to the presence of glauconite in these samples. In some cases, glauconite was observed coating and infilling foraminiferal tests. On the basis of elevated Fe/Ca ratios >1.5 mmol mol^{-1}, three samples were rejected from further consideration (supporting information Figure S3).

Replicate measurements on separately picked, non-reductively cleaned specimens of Group I were performed on 102 samples showing an average standard deviation of 0.23 mmol mol^{-1} for Mg/Ca ratios. In detail, average standard deviation as a measure of natural intraspecies variability was 0.19 mmol mol^{-1} for *G. ruber* (±4%; n = 14), 0.22 mmol mol^{-1} for *G. sacculifer* (±5%; n = 20), 0.11 mmol mol^{-1} for *G. cultrata* (±3%; n = 9), 0.41 mmol mol^{-1} for *P. obliquiloculata* (±13%; n = 8), 0.20 mmol mol^{-1} for *N. dutertrei* (±6%; n = 13), 0.20 mmol mol^{-1} for *G. menardii* (±7%; n = 23), 0.06 mmol mol^{-1} for *G. scitula* (±3%; n = 4), and 0.40 mmol mol^{-1} for *G. truncatulinoides* d. (±13%; n = 11).

Calculation of the calcite-saturation state $\Delta[CO_3^{2-}]$ was accomplished via subtracting carbonate-ion concentration ($[CO_3^{2-}]$) at saturation [*Jansen et al.*, 2002] from in situ $[CO_3^{2-}]$. The latter is available for the SCS from the SouthEast Asian Time-series Study (SEATS) station located in the northern SCS [*Chou et al.*, 2007]. For computing world ocean in situ $[CO_3^{2-}]$ with the program co2sys [*Lewis and Wallace*, 1998] using K_1 and K_2 after *Mehrbach et al.* [1973] refitted by *Dickson and Millero* [1987] and K_{SO4} after *Dickson* [1990], we used total alkalinity, TCO_2 (sum of dissolved CO_2, HCO_3^-, and CO_3^{2-}), pCO_2 (partial pressure of CO_2), pH, and hydrographic water-column data obtained from the World Ocean Circulation Experiment (lines illustrated in the supporting information Figure S4; data available from 6,320 stations with more than 98,000 water samples at http://woce.nodc.noaa.gov/wdiu).

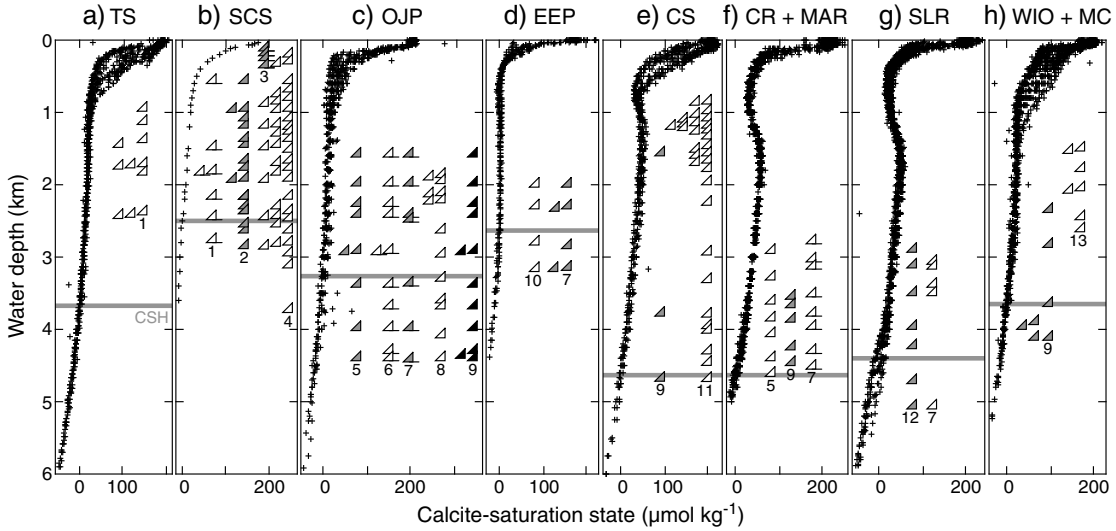

Figure 4. Water column profiles of $\Delta[CO_3^{2-}]$ (crosses) from 10 ocean regions (Table 2). Arrowheads, arbitrarily positioned with respect to $\Delta[CO_3^{2-}]$ values (*x* axis), indicate water depths of sediment-surface samples with Mg/Ca ratios of various planktonic foraminiferal species. Numbers 1–13 indicate the study from which the data sets were obtained. Reasonable calcite-saturation states are taken from the shown profiles if not available from the respective studies [*Rosenthal and Boyle*, 1993; *Russell et al.*, 1994; *Lea et al.*, 2000; *Whitko et al.*, 2002; *Steinke et al.*, 2005; *Mekik and François*, 2006; *Regenberg et al.*, 2010; *Xu et al.*, 2010; *Fallet et al.*, 2012].

We compared our SCS Mg/Ca ratios to 63 multispecies planktonic foraminiferal surface-sediment Mg/Ca data sets from 10 Pacific, Atlantic, and Indian Ocean regions (supporting information Figure S4; in total 758 Mg/Ca ratios) with relatively uniform intraregional temperatures within foraminiferal habitats, excluding data sets from the same studies with unreasonably high Mg/Ca ratios such as *G. ruber* (2.61–12.27 mmol mol^{-1}) and *Orbulina universa* (3.17–7.49 mmol mol^{-1}) data from *Russell et al.* [1994]. $\Delta[CO_3^{2-}]$ at the bottom water-sediment interface (Figure 4) was obtained from the computed profiles of $\Delta[CO_3^{2-}]$ (Table 2) if not available from the respective studies [*Fallet et al.*, 2012; *Lea et al.*, 2000; *Mekik and François*, 2006; *Regenberg et al.*, 2010; *Rosenthal and Boyle*, 1993; *Russell et al.*, 1994; *Steinke et al.*, 2005; *Whitko et al.*, 2002; *Xu et al.*, 2010]. 63 Mg/Ca ratios from samples exposed to bottom waters with $\Delta[CO_3^{2-}]$ between 30 and 40 μmol kg^{-1} [*Dekens et al.*, 2002; *Johnstone et al.*, 2011; *Regenberg et al.*, 2006; *Russell et al.*, 1994] were omitted from further consideration to distinguish between samples clearly affected and unaffected by dissolution. Cleaning of foraminiferal tests included [*Dekens et al.*, 2002; *Lea et al.*, 2000; *Rosenthal and Boyle*, 1993; *Russell et al.*, 1994; *Xu et al.*, 2010] or excluded reductive steps [*Brown and Elderfield*, 1996; *Fallet et al.*, 2012; *Johnstone et al.*, 2011; *Mekik and François*, 2006; *Regenberg et al.*, 2006, 2010; *Steinke et al.*, 2005; *Whitko et al.*, 2002].

Table 2. Spatial Extents of Ocean Regions With Sediment-Surface Planktonic Foraminiferal Mg/Ca Studies (Figure 4) for Selecting Calcite-Saturation States of Overlying Bottom Waters

	Longitude		Latitude		Calcite-Saturation
Ocean Region	Minimum	Maximum	Minimum	Maximum	Horizon, Depth (km)
South China Sea (SCS), SEATS station	115.58°E		18.25°N		2.5
Ontong Java Plateau (OJP)	144.81°E	165.02°E	4.3597°S	11.161°N	3.2
Eastern Equatorial Pacific (EEP)	85.82°W	92.58°W	11.49°S	12.224°N	2.6
Caribbean Sea (CS)	64.75°W	66.02°W	11.001°N	20.024°N	4.7
Ceara Rise (CR)	37.67°W	51.56°W	0.3912°N	13.662°N	4.7
Sierra Leone Rise (SLR)	12.5°W	28.75°W	8.0683°S	10.5°N	4.4
Mid-Atlantic Ridge (MAR)	37.67°W	51.56°W	0.3912°N	13.662°N	4.7
Mozambique Channel (MC)	35.365°E	48.886°E	24.675°S	4.0528°S	3.7
Western Indian Ocean (WIO)	45.499°E	54.109°E	33.515°S	7.518°S	3.7
Timor Sea (TS)	105.63°E	112.77°E	24.782°S	9.0042°S	3.7

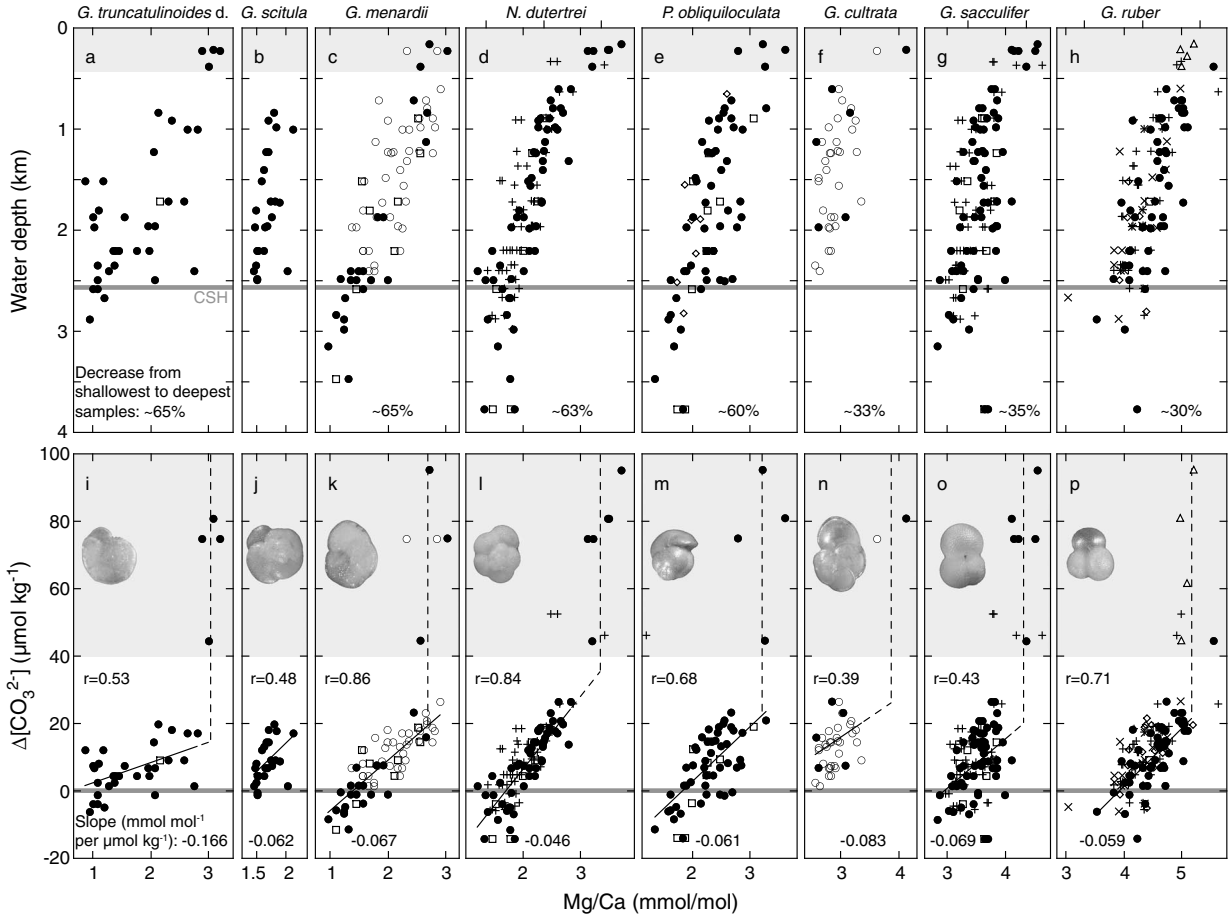

Figure 5. Species-specific Mg/Ca ratios of planktonic foraminifera (intermediate diameter of photographs 315–355 μm) from SCS sediment-surface samples (this study: filled circles (Group I), open squares (Group II), pluses (Group III); *Whitko et al.* [2002]: crosses; *Steinke et al.* [2005]: triangles; *Regenberg et al.* [2010]: open circles; *Xu et al.* [2010]: open diamonds) decrease with (a–h) increasing depositional water depth and (i–p) decreasing calcite-saturation states of overlying bottom waters adopted from SEATS station [*Chou et al.*, 2007]. Shaded areas illustrate well supersaturated bottom waters with $\Delta[CO_3^{2-}]>40$ μmol kg^{-1} at water depths <400 m, where Mg/Ca ratios are stable. Relative Mg/Ca decreases from shallowest to deepest samples and absolute declines of Mg/Ca ratios from <30 μmol kg^{-1} (regression lines through non-reductively cleaned samples from this study and *Regenberg et al.* [2010]) are indicated. Dashed vertical lines represent mean non-reductively cleaned Mg/Ca ratios from <40 μmol kg^{-1} [this study; *Steinke et al.*, 2005; *Regenberg et al.*, 2010]. Horizontal lines represent the position of the calcite-saturation horizon. Note that each Mg/Ca ratio of Group III (pluses) was corrected by +0.3 mmol mol^{-1} before plotting.

4. Results

The majority of our Mg/Ca data is assembled in Group I (Table 1) and shows patterns and trends representative of all data sets from the South China Sea (Figure 5). In detail, the 313 non-reductively cleaned SCS planktonic foraminiferal Mg/Ca ratios of Group I complemented by other data from the SCS (75 samples from *Regenberg et al.* [2010] and *Steinke et al.* [2005]) range from 0.87 to 5.09 mmol mol^{-1} (Figure 5; supporting information Table S1). As expected, the mixed-layer dwellers show highest Mg/Ca ratios (*G. ruber* 3.52–5.55 mmol mol^{-1}, *G. sacculifer* 2.82–4.55 mmol mol^{-1}, and *G. cultrata* 2.54–4.13 mmol mol^{-1}) followed by the thermocline dwellers (*P. obliquiloculata* 1.35–3.59 mmol mol^{-1}, *N. dutertrei* 1.21–3.70 mmol mol^{-1}, and *G. menardii* 0.96–3.01 mmol mol^{-1}) and the subthermocline dwellers (*G. scitula* 1.44–2.13 mmol mol^{-1}, *G. truncatulinoides* d. 0.87–3.19 mmol mol^{-1}). Such variations are larger than expected from temperature variations within a respective foraminiferal habitat (Figures 2 and 3).

For each group of data sets, SCS Mg/Ca ratios of each species reveal decreasing trends with water depth (Figures 5a–5h). From the shallowest to the deepest samples, Mg/Ca ratios decrease by 30–35% in mixed-layer dwellers (Figures 5f–5h) and 60–65% in (sub-)thermocline species (Figures 5a–5e). Higher relative decreases for (sub-)thermocline species are due to their lower absolute Mg/Ca ratios and hint at comparable absolute declines in Mg/Ca ratios for all species. In comparison with relatively invariant

temperatures at the different habitat-depth levels with temperature differences between northern and southern SCS stations of ≈2.6°C (Figures 2 and 3), intraspecific Mg/Ca variability (Figures 5a–5h) is too high to be explained by temperature alone. Conversion to temperatures with standard calibrations [e.g., *Lea et al.*, 2000; *Dekens et al.*, 2002; *Anand et al.*, 2003] translates the scatter of Mg/Ca ratios to temperature variations of about 4.1°C for *G. ruber*, 5.2°C for *G. sacculifer*, 3.9°C for *G. cultrata*, 9.8°C for *P. obliquiloculata*, 10.8°C for *N. dutertrei*, 12.7°C for *G. menardii*, 4.4°C for *G. scitula*, and 14.4°C for *G. truncatulinoides* d.

Rapid drop of SCS $\Delta[CO_3^{2-}]$ within the upper hundreds of meters, where waters are fairly supersaturated (≈180 − −40 μmol kg^{-1}) with respect to calcite, becomes gradual below about 700 m (Figure 4b). While Mg/Ca ratios from shallow sites are exempt from decreasing trends, apparently decreasing Mg/Ca ratios are positively correlated with $\Delta[CO_3^{2-}]$ of bottom waters close to and below saturation (Figures 5i–5p). Instead of presenting relative decreases, which are higher for (sub-)thermocline dwellers with low absolute Mg/Ca ratios (Figures 5a–5h), we obtained absolute declines in Mg/Ca ratios (Figures 5i–5p). Below 30 μmol kg^{-1}, the mean decline (within the given uncertainty interval) in non-reductively cleaned Mg/Ca ratios of Group I per μmol kg^{-1} is 0.058 (0.051–0.068) mmol mol^{-1} for *G. ruber*, 0.069 (0.054–0.096) mmol mol^{-1} for *G. sacculifer*, 0.083 (0.059–0.138) mmol mol^{-1} for *G. cultrata*, 0.061 (0.053–0.072) mmol mol^{-1} for *P. obliquiloculata*, 0.046 (0.042–0.051) mmol mol^{-1} for *N. dutertrei*, 0.067 (0.062–0.073) mmol mol^{-1} for *G. menardii*, 0.062 (0.045–0.100) mmol mol^{-1} for *G. scitula*, and 0.166 (0.127–0.239) mmol mol^{-1} for *G. truncatulinoides* d. (supporting information Table S1).

5. Discussion

5.1. Causes of Mg/Ca Variations

We present Mg/Ca ratios from the South China Sea measured following different cleaning protocols and analytical setups (Table 1). While the small difference of about 3% between Group I and II (different cleaning protocols, ICP-OES analysis at IfG) suggest minor influence of the reductive step on SCS Mg/Ca ratios, Group III (reductively cleaned, ICP-MS analysis at UCSB) is lower by ≈0.3 mmol mol^{-1} (Figure 5). This offset can be due to (1) size-related inhomogeneity of Mg/Ca ratios between the size fractions used, which was reported to be in the order of 0.2 mmol mol^{-1} [*Elderfield et al.*, 2002], and (2) different standardization with deviations of up to 0.1 mmol mol^{-1} between laboratories [*Rosenthal et al.*, 2004]. Because we are not able to precisely establish the cause of the offset, we plot the Group III data offset by 0.3 mmol mol^{-1} by including a +0.3 mmol mol^{-1} correction for all Group III data to harmonize the data sets (Figure 5). Patterns and trends, however, are similar for all Mg/Ca data sets of each group. Neither of the SCS Mg/Ca data sets (nor of the available Mg/Ca data sets from other ocean areas) convincingly reflects the relatively uniform temperatures within the foraminiferal habitats (Figures 2 and 3), suggesting dissolution to be the driving force of declines in Mg/Ca ratios.

5.1.1. Dissolution-Unaffected Mg/Ca Ratios

Foraminiferal tests from shallow southern SCS samples <400 m water depth were exposed to bottom waters supersaturated with respect to calcite ($\Delta[CO_3^{2-}]$ >40 μmol kg^{-1}, Figures 4b and 5). Their Mg/Ca ratios do not systematically vary with bottom water $\Delta[CO_3^{2-}]$ and slightly deviate by about ±10% from species-specific means. Like Caribbean and Indian Ocean samples exposed to $\Delta[CO_3^{2-}]$ >40 μmol kg^{-1} [*Johnstone et al.*, 2011; *Regenberg et al.*, 2006; *Sadekov et al.*, 2010], these shallow SCS Mg/Ca ratios can be assumed to be dissolution-unaffected. In the thermally invariant southern SCS, where spatial temperature variation at species-specific habitat depths is small (Figure 3), the mean Mg/Ca ratios from samples <400 m water depth (Figures 5a–5h) resemble species-specific initial Mg/Ca ratios.

With some reservations, southern SCS mean Mg/Ca ratios also serve as benchmarks for the respective species from the northern SCS, where shallow water samples are unavailable. Converting annual temperature differences at similar depth levels between the southern and northern SCS sites (Figures 2 and 3) to variations in Mg/Ca ratios with standard calibrations [e.g., *Anand et al.*, 2003; *Lea et al.*, 2000], the temperature-induced intraspecific scatters should not exceed 1.2 mmol mol^{-1} for mixed-layer and thermocline dwellers and 0.4 mmol mol^{-1} for deep dwellers.

5.1.2. Intraspecific Mg/Ca Variation

Focusing on intraspecific Mg/Ca variation at similar sample water depths >400 m, differences between highest and lowest Mg/Ca ratios of about 1.2 mmol mol^{-1} of mixed-layer and thermocline dwellers (Figure 5) can be explained as temperature-induced scatter. Such high Mg/Ca scatter might partly also result from vertical migration of shallow- and thermocline-dwelling species during their ontogenetic cycles [e.g., *Duplessy et al.*,

1981; *Regenberg et al.*, 2010; *Schiebel and Hemleben*, 2005], which integrates temperatures recorded during chamber formation at different water depths levels.

Highest intraspecific Mg/Ca variation of about 1.8 mmol mol^{-1} at similar sample depths is observed for deep-dwelling *G. truncatulinoides* d. Converted with standard calibrations, its calcification temperatures vary by about 11°C, which is much more than highest differences between SCS stations at similar water depths within the deep habitat realm (Figures 2 and 3). Because *G. truncatulinoides* tracks an ontogenetic cycle with enormous vertical migration of several hundreds of meters [*LeGrande et al.*, 2004; *Mulitza et al.*, 1997], its Mg/Ca ratio integrates temperature signals from different levels of the permanent thermocline [*McKenna and Prell*, 2004]. We thus ascribe the relatively high Mg/Ca scatter to already varying initial Mg/Ca ratios, which were recorded during subsequent chamber formation at different apparent calcification depths within permanent thermocline waters [*Anand et al.*, 2003; *LeGrande et al.*, 2004; *Lončarić et al.*, 2006; *Regenberg et al.*, 2009].

5.2. Dissolution Effects on Mg/Ca Ratios Revisited

Despite the intraspecific Mg/Ca variation at similar sample depths, there is an apparent decline of SCS Mg/Ca ratios with increasing depositional water depth (Figures 5a–5h). This pattern is similar to continuously decreasing Mg/Ca ratios with increasing water depths of foraminiferal test deposition from eastern Equatorial Pacific (EEP) sediment-surface samples [*Lea et al.*, 2000] but contrasts with Caribbean Sea (CS) preservation of initial Mg/Ca ratios down to water depths of about 2500 m [*Regenberg et al.*, 2006]. The pattern of how $\Delta[CO_3^{2-}]$ affects SCS Mg/Ca ratios is comparable to the CS [*Regenberg et al.*, 2006]: dissolution-unaffected samples can be assigned to fairly supersaturated waters with respect to calcite, whereas dissolution-affected samples can be found below certain $\Delta[CO_3^{2-}]$ values. Our SCS results reconcile the seemingly inconsistent interpretations of the continuously decreasing EEP Mg/Ca ratios with increasing water depth with the discontinuous effect reported from CS sediment-surface samples [*Lea et al.*, 2000; *Regenberg et al.*, 2006]. This supports the suggested direct link between dissolution effects on Mg/Ca ratios and $\Delta[CO_3^{2-}]$ of bottom waters [*Brown and Elderfield*, 1996; *Dekens et al.*, 2002; *Johnstone et al.*, 2011; *Regenberg et al.*, 2006]. Based on Mg/Ca data sets from different ocean regions (Figure 4; Table 2), we will subsequently establish that Mg/Ca ratios are subject to dissolution below a certain $\Delta[CO_3^{2-}]$ threshold and that continuous declines in Mg/Ca ratios are similar for the different foraminiferal species.

5.2.1. Onset of Mg/Ca Dissolution

To quantify the $\Delta[CO_3^{2-}]$ value, below which dissolution effects on SCS Mg/Ca ratios start, linear regressions were calculated for species-specific Mg/Ca ratios from samples <30 μmol kg^{-1} (Figures 5i–5p). Where these regression lines intercept mean species-specific Mg/Ca ratios representative of the initial Mg/Ca signal (calculated from samples >40 μmol kg^{-1}; Figures 5i–5p), critical thresholds for the onset of Mg/Ca dissolution are defined [*Regenberg et al.*, 2006]. Table 3 summarizes the SCS critical thresholds and those derived from 18 Mg/Ca data sets from the Ceara Rise (CR) and CS available in the literature including samples exposed to both bottom waters with $\Delta[CO_3^{2-}]$ >40 μmol kg^{-1} (supporting information Table S2) and <30 μmol kg^{-1} (supporting information Table S1). Mg/Ca ratios from bottom waters with $\Delta[CO_3^{2-}]$ between 30 and 40 μmol kg^{-1} were excluded from further consideration because they do not clearly belong to the dissolution-unaffected or dissolution-affected group. Thresholds range from 7.0 to 35.6 μmol kg^{-1} with a mean $\Delta[CO_3^{2-}]$ of 22.4 ±6.5 μmol kg^{-1} for the onset of dissolution within overlapping uncertainty intervals (Table 3). Similar threshold values can be calculated for shallow (20.7 μmol kg^{-1}), intermediate (24.6 μmol kg^{-1}), and deep dwellers (22.7 μmol kg^{-1}) or for data sets from the SCS (21.7 μmol kg^{-1}), CR (26.4 μmol kg^{-1}), and CS (21.3 μmol kg^{-1}). Differences between species, ocean regions, and studies do thus not appear to reflect a distinct and significant pattern.

5.2.2. Decline in Mg/Ca Ratios

As analogous to the SCS (Figure 5), ocean regions with relatively invariant temperatures within a planktonic foraminiferal habitat reveal dissolution-induced declines in Mg/Ca ratios. Declines of Mg/Ca ratios can be estimated from the slopes of regression lines through samples exposed to bottom waters with $\Delta[CO_3^{2-}]$ <30 μmol kg^{-1}. Recalculated from the original Mg/Ca ratios, available 79 Mg/Ca data sets of multiple foraminiferal species from the SCS [*Regenberg et al.*, 2010; *Whitko et al.*, 2002; *Xu et al.*, 2010], Ontong Java Plateau [OJP; *Brown and Elderfield*, 1996; *Dekens et al.*, 2002; *Johnstone et al.*, 2011; *Mekik and François*, 2006; *Russell et al.*, 1994], EEP [*Dekens et al.*, 2002; *Lea et al.*, 2000], CS [*Johnstone et al.*, 2011; *Regenberg et al.*, 2006], CR [*Dekens et al.*, 2002; *Russell et al.*, 1994], Mid-Atlantic Ridge [MAR; *Johnstone et al.*, 2011], Sierra Leone Rise [SLR; *Dekens et al.*, 2002; *Rosenthal and Boyle*, 1993], Mozambique Channel [MC; *Fallet et al.*,

Table 3. Available Mg/Ca Data Sets With Sediment-Surface Samples Exposed to Both Bottom Waters With $\Delta[CO_3^{2-}]$ >40 μmol kg^{-1} and <30 μmol kg^{-1} [a]

Species	Study	Ocean Region	Number of Samples >40	Number of Samples <30	Calcite-Saturation Threshold (μmol kg^{-1})	Uncertainty Interval (μmol kg^{-1})
		Shallow Dweller				
G. ruber	*Johnstone et al.* [2011]	CS	1	2	7.0	ND
G. ruber	*Dekens et al.* [2002]	CR	1	5	16.9	−25.5–59.2
G. ruber	Group III	SCS	2	44	17.9	4.2–31.6
G. ruber	*Steinke et al.* [2005]; Group I	SCS	5	50	21.6	8.8–34.4
G. ruber	*Regenberg et al.* [2006]	CS	26	10	25.4	−4.8–55.6
G. ruber p.	*Regenberg et al.* [2006]	CS	24	10	30.2	14.5–45.9
G. sacculifer	*Johnstone et al.* [2011]	CS	1	2	11.1	n.d.
G. sacculifer	Group III	SCS	4	54	15.5	1.5–29.5
G. sacculifer	*Regenberg et al.* [2006]	CS	27	12	20.2	−16.2–56.5
G. sacculifer	Group I	SCS	6	57	20.2	2.5–37.9
G. sacculifer	*Russell et al.* [1994]	CR	3	10	25.4	−9.9–60.8
G. sacculifer	*Dekens et al.* [2002]	CR	1	5	32.2	−50.3–115
G. cultrata	*Regenberg et al.* [2010]; Group I	SCS	2	36	25.4	6.6–44.2
		Intermediate Dweller				
N. dutertrei	*Johnstone et al.* [2011]	CS	1	2	23.3	ND
N. dutertrei	Group III	SCS	3	55	24.0	18.0–30.0
N. dutertrei	*Regenberg et al.* [2006]	CS	24	11	28.1	7.0–49.2
N. dutertrei	*Dekens et al.* [2002]	CR	1	5	30.6	21.2–40.1
N. dutertrei	Group I	SCS	7	50	35.6	28.8–42.4
P. obliquiloculata	*Johnstone et al.* [2011]	CS	1	2	13.8	ND
P. obliquiloculata	Group I	SCS	4	49	22.7	14.5–30.9
G. menardii	*Regenberg et al.* [2010]; Group I	SCS	5	58	19.6	16.4–22.8
G. menardii	*Regenberg et al.* [2006]	CS	25	8	23.8	3.0–44.6
		Deep Dweller				
G. tumida	*Regenberg et al.* [2006]	CS	16	10	19.0	−3.6–41.7
G. tumida	*Russell et al.* [1994]	CR	5	14	27.0	22.0–32.0
G. truncatulinoides d.	Group I	SCS	4	30	14.7	9.1–20.3
G. truncatulinoides d.	*Regenberg et al.* [2006]	CS	22	7	22.6	3.1–42.2
G. truncatulinoides s.	*Regenberg et al.* [2006]	CS	5	7	27.4	−11.2–65.9
G. crassaformis	*Regenberg et al.* [2006]	CS	10	10	25.2	5.4–45.0
Mean					22.4 ± 6.5	

[a] $\Delta[CO_3^{2-}]$ thresholds (μmol kg^{-1}) are valid within their respective uncertainty intervals deduced from standard errors of linear regressions of $\Delta[CO_3^{2-}]$ on Mg/Ca ratios. ND means no data.

2012], Western Indian Ocean [WIO; *Johnstone et al.*, 2011], and Timor Sea [TS; *Xu et al.*, 2010] surface sediments show linearly declining Mg/Ca ratios with increasing water depth and decreasing $\Delta[CO_3^{2-}]$ of bottom waters (except for SCS *G. ruber* [*Xu et al.*, 2010], OJP *G. sacculifer* [*Russell et al.*, 1994], and MC *N. dutertrei* [*Fallet et al.*, 2012]; supporting information Table S1). Uncertainty intervals of the declines in Mg/Ca ratios deduced from standard errors of the linear regressions of $\Delta[CO_3^{2-}]$ on Mg/Ca ratios are largely overlapping.

The exponential dependence of the Mg/Ca increase on temperature during test formation [e.g., *Anand et al.*, 2003; *Lea et al.*, 2000; *Regenberg et al.*, 2009] causes interspecies and interregional differences between initial Mg/Ca ratios. The only Mg/Ca data sets directly comparable to each other are those measured on the same foraminiferal species from the same ocean region, because those tests experienced roughly the same Mg^{2+} incorporation due to similar temperatures in their habitat depth (e.g., SCS *G. ruber* Mg/Ca ratios of Group I and *Whitko et al.* [2002] with average declines per μmol kg^{-1} (within overlapping uncertainty intervals) of 0.058 (0.051–0.068) mmol mol^{-1} and 0.073 (0.060–0.093) mmol mol^{-1}, respectively). Additionally, Mg/Ca variation between studies may result from methodological differences such as size-related intraspecies variations [e.g., *Elderfield et al.*, 2002; *Friedrich et al.*, 2012], different cleaning protocols [e.g., *Barker et al.*, 2003; *Martin and Lea*, 2002], and different analytical setups [e.g., *Rosenthal et al.*, 2004]. Last but not least, single Mg/Ca data sets are limited in sample numbers and by narrow ranges of bottom water $\Delta[CO_3^{2-}]$ (Figure 4) further restricting the comparability of Mg/Ca data sets. Higher scattering of original Mg/Ca data sets thus results in larger uncertainty intervals (supporting information Table S1). Observed differences between declines (i.e., slopes) in Mg/Ca ratios from bottom waters with $\Delta[CO_3^{2-}]$ <30 μmol kg^{-1}, which are usually in

the range of 0.02–0.17 mmol mol^{-1} per μmol kg^{-1} (supporting information Table S1), cannot be interpreted as dissolution patterns dependent on the species and ocean region.

5.3. Normalization of Mg/Ca Data Sets

A prerequisite for a further interpretation of dissolution effects on planktonic foraminiferal Mg/Ca ratios is to test the direct comparability of the available Mg/Ca data sets. As discussed in the previous section, interspecies, interregional, and methodological differences cause offsets between Mg/Ca data sets preventing their combination. Offsets between Mg/Ca data sets can be removed by translation of each mean to zero and scaling of the standard deviation to 1 and −1, respectively (supporting information Figure S5). This normalization removes the thermal differences between species and regions as well as methodological differences between studies by adjusting all Mg/Ca ratios to a common and dimensionless scale. Separate normalization of each data set by its standard deviation after subtracting the mean ensures equal weight of all data sets [e.g., *Keenlyside et al.*, 2007; *Vautard and Ghil*, 1989]. Hence, we separately normalized Mg/Ca ratios ($Mg/Ca_{normalized}$) for each species, region, and study following equation (1):

$$Mg/Ca_{normalized} = (Mg/Ca_{observed} - Mg/Ca_{mean})/stdev. \quad (1)$$

The mean Mg/Ca ratio (Mg/Ca_{mean}) and standard deviation (stdev) of each data set (supporting information Table S3) was calculated from all its measured Mg/Ca ratios ($Mg/Ca_{observed}$) from bottom waters with $\Delta[CO_3^{2-}]$ <30 μmol kg^{-1}. Mg/Ca ratios from >40 μmol kg^{-1} were normalized by using Mg/Ca_{mean} and stdev from <30 μmol kg^{-1} of the same data set. Two SCS Mg/Ca data sets of Group I with 50 samples from <30 μmol kg^{-1} each exemplify this normalization approach: mean Mg/Ca ratios equal 2.08 mmol mol^{-1} for thermocline-dwelling *N. dutertrei* with a standard deviation of 0.41 mmol mol^{-1} and 4.51 mmol mol^{-1} for shallow-dwelling *G. ruber* with a standard deviation of 0.37 mmol mol^{-1} (supporting information Table S3). After applying equation (1), normalized Mg/Ca ratios are adjusted to a common and dimensionless scale so that *N. dutertrei* and *G. ruber* data are directly comparable. Student's *t* test determined the difference between both data sets to be insignificant (probability $P = 0.19$; $P > 0.05$ refutes the null hypothesis that the two Mg/Ca data sets are significantly different). Merging both normalized data sets, the decline in Mg/Ca ratios dependent on the bottom water $\Delta[CO_3^{2-}]$ can be determined on the basis of 100 samples. Above 40 μmol kg^{-1}, the *N. dutertrei* data set contains seven samples (supporting information Table S2), while one *G. ruber* Mg/Ca ratio was complemented by four Mg/Ca ratios from *Steinke et al.* [2005]. These initial Mg/Ca ratios were normalized to the means and standard deviations from <30 μmol kg^{-1} and are combinable ($P = 0.84$) to derive a significant initial mean based on 12 values.

Such normalized data sets are beneficial to check for Mg/Ca dissolution dependencies on the foraminiferal species and the ocean region. Combination of all normalized Mg/Ca data sets enables a statistically robust validation of calcite-dissolution effects on Mg/Ca ratios within their respective uncertainties based on a maximum data set of in total 1265 Mg/Ca ratios. Student's *t* test determined differences between the 79 normalized Mg/Ca data sets from <30 μmol kg^{-1} (in total 1027 Mg/Ca ratios) of the various species, ocean regions, and studies to be insignificant (probability *P* at least 0.06, except for the five data pairs: CS *N. dutertrei* [*Regenberg et al.*, 2006] compared with (a) SCS Group I *G. sacculifer* ($P = 0.045$), (b) OJP *G. sacculifer* [*Russell et al.*, 1994] ($P = 0.044$), and (c) SCS Group III *G. ruber* ($P = 0.031$); SCS Group I *G. truncatulinoides* d. compared with (a) SCS Group I *G. sacculifer* ($P = 0.036$) and (b) SCS Group III *G. ruber* ($P = 0.024$). Differences between the 28 Mg/Ca data sets containing in total 235 Mg/Ca ratios from >40 μmol kg^{-1} (supporting information Table S2) are insignificant without exception. This result implies that normalized initial Mg/Ca ratios >40 μmol kg^{-1} are similar and combinable, and declines in Mg/Ca ratios <30 μmol kg^{-1} are indistinguishable. Previously suggested decreases in Mg/Ca ratios dependent on ocean basin or foraminiferal species [e.g., *Brown and Elderfield*, 1996; *Dekens et al.*, 2002; *Rosenthal and Linsley*, 2007; *Rosenthal and Lohmann*, 2002] are statistically insignificant and therefore appear unlikely. Consequently, merging of all Mg/Ca ratios into a normalized global data set makes it possible to quantify a general decline in Mg/Ca ratios and onset of Mg/Ca dissolution within their uncertainty intervals (Figure 6).

5.4. Global Dissolution Effects

Solving equation (1) for $Mg/Ca_{observed}$ using normalized Mg/Ca ratios at two arbitrarily chosen $\Delta[CO_3^{2-}]$ levels on the regression line through the normalized Mg/Ca ratios (e.g., $Mg/Ca_{normalized}$ of −1.16 at 0 μmol kg^{-1} and $Mg/Ca_{normalized}$ of −1.32 at −1 μmol kg^{-1}, respectively; Figure 6), we recalculated linear declines in Mg/Ca ratios per μmol kg^{-1} for the 79 different data sets of each species, ocean region, and study using

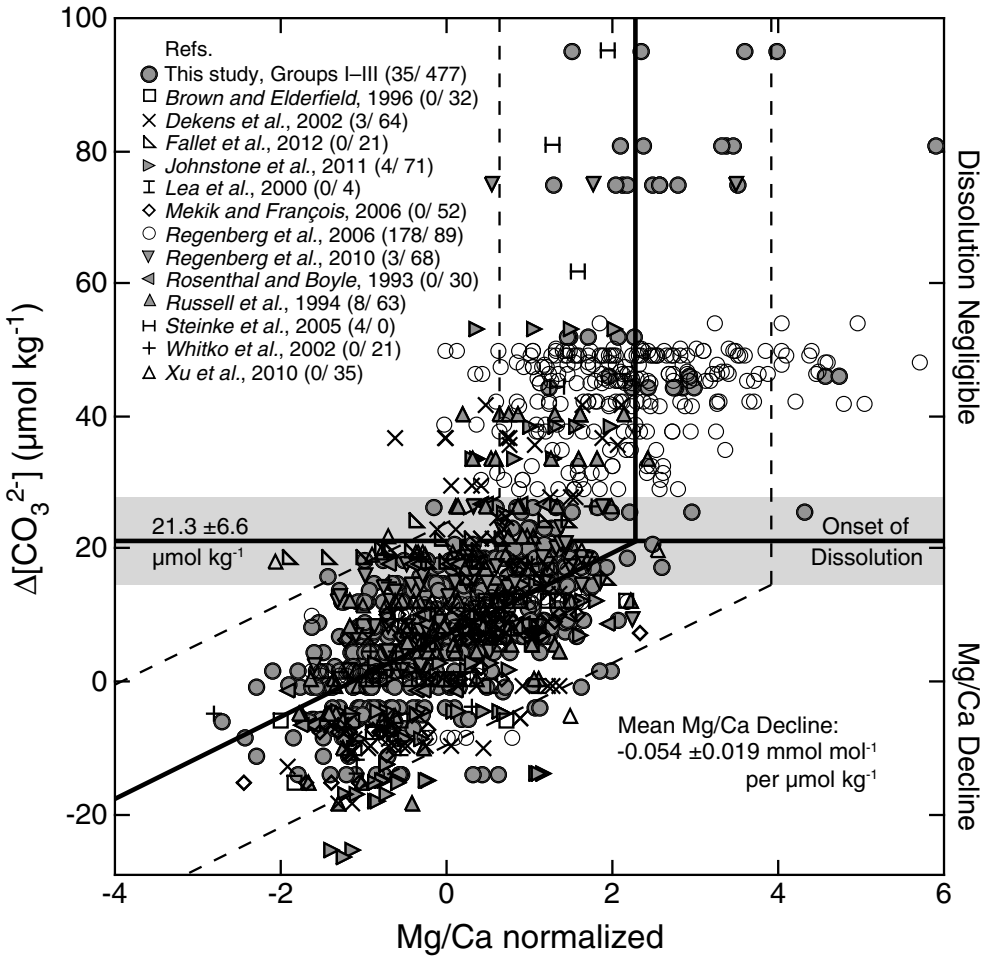

Figure 6. The dissolution pattern of 1262 normalized Mg/Ca ratios controlled by $\Delta[CO_3^{2-}]$ of bottom waters is characterized by the stability of initial Mg/Ca ratios down to the critical threshold of 21.3 ±6.6 µmol kg^{-1} (horizontal line ±shaded area). The critical calcite-dissolution threshold was determined by the intersection of the mean normalized Mg/Ca ratio (with uncertainty range, vertical lines) >40 µmol kg^{-1}, which is representative of each species and region (P >0.12), and the regression (±prediction interval with a 95% probability, diagonal lines) through normalized Mg/Ca ratios <30 µmol kg^{-1}. The regression line represents the mean decrease of normalized Mg/Ca ratios. Note that the 74 Mg/Ca ratios in the 30–40 µmol kg^{-1} interval are excluded from mean and regression calculations. Renormalization results in a mean decline in Mg/Ca ratios of 0.054 ± 0.019 mmol mol^{-1} per µmol kg^{-1} below the critical threshold (supporting information Table S3). Reference data sets [*Brown and Elderfield*, 1996; *Dekens et al.*, 2002; *Fallet et al.*, 2012; *Johnstone et al.*, 2011; *Lea et al.*, 2000; *Mekik and François*, 2006; *Regenberg et al.*, 2006, 2010; *Rosenthal and Boyle*, 1993; *Russell et al.*, 1994; *Steinke et al.*, 2005; *Whitko et al.*, 2002; *Xu et al.*, 2010] consist of given numbers of multispecies Mg/Ca measurements (>40/ <30 µmol kg^{-1}).

Mg/Ca_{mean} (supporting information Table S3). Declines in Mg/Ca ratios range from 0.015 to 0.175 mmol mol^{-1} per µmol kg^{-1} with a mean of 0.054 ± 0.019 mmol mol^{-1} per µmol kg^{-1} when excluding Mg/Ca data sets based on only two or three stations each (Figure 6 and supporting information Table S3). This absolute decline in Mg/Ca ratios dependent on the $\Delta[CO_3^{2-}]$ of overlying bottom waters is representative of all planktonic foraminiferal species and ocean regions and best approximates a fixed value being removed from Mg/Ca ratios during a change in bottom water $\Delta[CO_3^{2-}]$ of 1 µmol kg^{-1} below the critical $\Delta[CO_3^{2-}]$ threshold of 21.3 ±6.6 µmol kg^{-1} (Figure 6).

The fixed value of decline in Mg/Ca ratios below the $\Delta[CO_3^{2-}]$ threshold (Figure 6) implies a thermodynamic control on dissolution effects. It seems that the inhomogeneous distribution of Mg^{2+} throughout test chambers causes calcite with higher Mg/Ca ratios, which is more soluble, to be preferentially removed as already stated by *Brown and Elderfield* [1996]. The dissolution impact on Mg/Ca paleotemperature estimates is dependent on the species. For shallow dwellers with high initial Mg/Ca ratios >2.8 mmol mol^{-1} as indicators

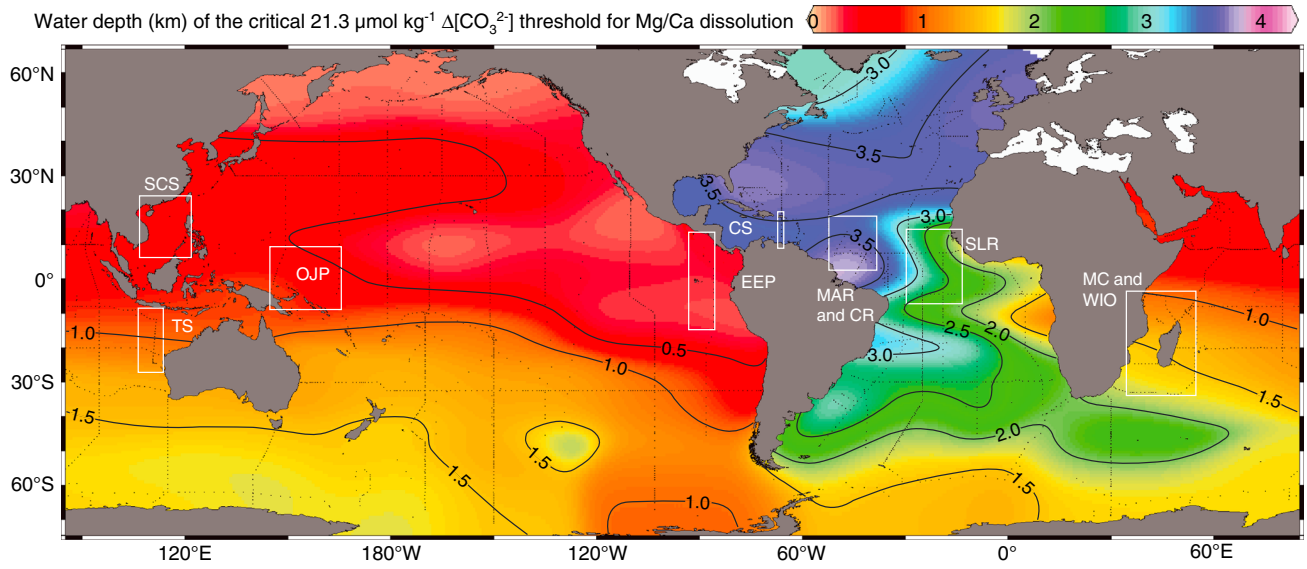

Figure 7. Global distribution of the 21.3 µmol kg^{-1} calcite-saturation state as critical threshold for the onset of calcite dissolution. Initial foraminiferal Mg/Ca ratios and hence reliable Mg/Ca paleotemperatures are preserved down to the illustrated water depths (contour lines in kilometer). Black dots represent World Ocean Circulation Experiment and SCS SEATS stations, from which data were extracted to calculate $\Delta[CO_3^{2-}]$ of the water column. Boxes indicate ocean regions with extracted calcite-saturation profiles (Figure 4 and Table 2).

of surface and mixed-layer temperatures, the relative decline in Mg/Ca ratios ranges between 1 and 2% per µmol kg^{-1}. Calculated paleotemperatures from such dissolution-affected foraminiferal Mg/Ca ratios underestimate the thermal conditions in their habitats by about 0.1–0.2°C per µmol kg^{-1}. In contrast, deep dwellers and (sub-)polar species lose 3–5% per µmol kg^{-1} of their Mg/Ca signal due to dissolution when initial Mg/Ca ratios are lower than 1.9 mmol mol^{-1}. Respective Mg/Ca paleotemperature underestimates of subthermocline and polar water masses are therefore on the order of 0.4–0.6°C per µmol kg^{-1}.

The global onset of dissolution effects on planktonic foraminiferal Mg/Ca ratios deduced from the normalized Mg/Ca data sets occurs at a critical $\Delta[CO_3^{2-}]$ threshold of 21.3 ±6.6 µmol kg^{-1} (Figure 6). The water depth of this critical threshold for calcite dissolution shoals from more than 3.5 km in the North Atlantic Ocean to less than 0.5 km in the North Pacific Ocean (Figure 7). It varies throughout the oceans like the depth of the calcite-saturation horizon (Figure 4) as result of cumulative enrichment of dissolved total organic carbon relative to total alkalinity in intermediate and deep waters of the Indian and Pacific Oceans in comparison with the Atlantic Ocean [e.g., *Feely et al.*, 2004]. However, critical water depths for planktonic foraminiferal Mg/Ca paleotemperatures, where estimates fall outside the calibration uncertainties [*Anand et al.*, 2003; *Dekens et al.*, 2002; *Regenberg et al.*, 2009] and are thus unreliable, are again dependent on the species. Paleotemperatures reconstructed from shallow dwellers require correction when tests were deposited about 800 m below the calcite-dissolution threshold. For deep dwellers and polar species, critical water depths are reached about 200 m below the threshold. Above this critical threshold dissolution effects on planktonic foraminiferal Mg/Ca ratios are negligible.

The global value of decline in Mg/Ca ratios valid for all planktonic foraminiferal species (0.054 mmol mol^{-1} per µmol kg^{-1} below the critical $\Delta[CO_3^{2-}]$ threshold of 21 µmol kg^{-1}; Figure 6) provides a comprehensive basis for the correction of Mg/Ca paleotemperature estimates affected by dissolution in bottom waters. So far, a correction routine for downcore temperature estimates developed by *Dekens et al.* [2002] can be applied to compensate for dissolution effects on Mg/Ca ratios assumed to be related to the depositional water depth of the samples. Applying this depths correction to a suite of latitudinally distributed cores from the Atlantic Ocean, *Arbuszewski et al.* [2010] overcorrected Mg/Ca ratios from cores located in the subtropical North Atlantic relative to those from the eastern tropical Atlantic [*Hertzberg and Schmidt*, 2013]. Intrabasin variations in the depth of the critical threshold for the onset of Mg/Ca dissolution (i.e., up to 2.0 km in the Atlantic Ocean; Figure 7) indicate the need for correcting dissolution-affected Mg/Ca ratios only for the $\Delta[CO_3^{2-}]$ induced decline in order to obtain reliable paleotemperature estimates.

The general pattern of dissolution effects on Mg/Ca ratios dependent on bottom water $\Delta[CO_3^{2-}]$ can be obscured by other factors. Metabolic dissolution in response to respiration of organic matter in sediments [*Archer et al.*, 1989; *de Villiers*, 2005; *Martin and Sayles*, 2003] may decrease foraminiferal Mg/Ca ratios even at water depths above the $\Delta[CO_3^{2-}]$ threshold. Below the critical threshold, rapid burial of foraminiferal tests as a result of high sedimentation rates may protect the tests from dissolution through equilibration of pore waters with respect to calcite. These two processes are likely to cause some scatter in the planktonic foraminiferal Mg/Ca data sets but their impact remains unresolved without estimates of sedimentation and respiration rates. With respect to the modern and, more generally, interglacial calcite preservation in the deep oceans driven by $\Delta[CO_3^{2-}]$ of bottom waters, glacial Pacific-type preservation is enhanced, whereas Atlantic-type preservation is worse [e.g., *Dunn et al.*, 1981]. Related vertical migration of the calcite-saturation horizon by several hundreds of meters [e.g., *Broecker and Clark*, 2001; *Farrell and Prell*, 1989; *Fehrenbacher et al.*, 2006] should also significantly relocate the critical $\Delta[CO_3^{2-}]$ threshold of dissolution effects on planktonic foraminiferal Mg/Ca ratios. However, attempts to infer glacial bottom water $\Delta[CO_3^{2-}]$ [*Dunne et al.*, 2012; *Fehrenbacher and Martin*, 2011] suggest that the spatial deep-sea carbonate chemistry is more complex than uniform vertical shifting of $\Delta[CO_3^{2-}]$ levels within ocean basins.

6. Conclusions

We have demonstrated that Mg/Ca ratios of planktonic foraminiferal tests from globally distributed sediment-surface samples show a distinct preservation-dissolution pattern linked to $\Delta[CO_3^{2-}]$ of overlying bottom waters. The determined pattern is similar for each planktonic foraminiferal species. Initial Mg/Ca ratios recorded within a planktonic foraminiferal habitat are well preserved when deposited in bottom waters with $\Delta[CO_3^{2-}]$ above 21.3 ±6.6 μmol kg^{-1}. This critical threshold corresponds to water depths about 1.0–1.5 km shallower than the calcite-saturation horizon. Below this threshold Mg/Ca ratios in all species decrease by 0.054 ±0.019 mmol mol^{-1} per μmol kg^{-1}. Consequently, Mg/Ca-derived paleotemperatures from foraminiferal tests exposed to $\Delta[CO_3^{2-}]$ below the critical threshold are significantly underestimated by 0.1–0.2°C per μmol kg^{-1} for surface dwellers and 0.4–0.6°C per μmol kg^{-1} for subsurface and polar species.

Knowledge of bottom water $\Delta[CO_3^{2-}]$ at core sites located below the critical threshold offers the opportunity to recalculate initial planktonic foraminiferal Mg/Ca ratios from dissolution-affected tests by correcting for the 0.054 mmol mol^{-1} per μmol kg^{-1} decline. A detailed assessment of deep-sea $\Delta[CO_3^{2-}]$ is needed in order to reconstruct reliable Mg/Ca paleotemperature estimates for cores located close to or below the modern water depth of the critical $\Delta[CO_3^{2-}]$ threshold for the onset of dissolution effects on planktonic foraminiferal Mg/Ca ratios.

Acknowledgments
MR thanks Mareike Henneberg and Karin Kißling for laboratory assistance and technical support, and Anke Schneider and Douglas W. R. Wallace for guidance on running of the co2sys program. DWL gratefully acknowledges the technical support of John Horton (sample preparation) and Georges Paradis (ICP-MS analysis) at UCSB. We are grateful to Wolfgang Kuhnt and three anonymous reviewers for comments, and Wolfgang Kuhnt and Michael Sarnthein for providing samples and guidance in sample selection. This study was funded by the German Science Foundation through project RE 2901/2.

References

Anand, P., H. Elderfield, and M. H. Conte (2003), Calibration of Mg/Ca thermometry in planktonic foraminifera from sediment trap time series, *Paleoceanography*, *18*(2), 1050, doi:10.1029/2002PA000846.

Arbuszewski, J., P. deMenocal, A. Kaplan, and E. C. Farmer (2010), On the fidelity of shell-derived $\delta^{18}O_{seawater}$ estimates, *Earth. Planet. Sci. Lett.*, *300*, 185–196, doi:10.1016/j.epsl.2010.10.035.

Archer, D. E. (1996), An atlas of the distribution of calcium carbonate in sediments of the deep sea, *Global Biogeochem. Cycles*, *10*(1), 159–174.

Archer, D. E., S. Emerson, and C. Reimers (1989), Dissolution of calcite in deep-sea sediments: PH and O_2 microelectrode results, *Geochim. Cosmochim. Acta*, *53*(11), 2831–2845, doi:10.1016/0016-7037(89)90161-0.

Barker, S., M. Greaves, and H. Elderfield (2003), A study of cleaning procedures used for foraminiferal Mg/Ca paleothermometry, *Geochem. Geophys. Geosyst.*, *4*(9), 8407, doi:10.1029/2003GC000559.

Bian, N., and P. A. Martin (2010), Investigating the fidelity of Mg/Ca and other elemental data from reductively cleaned planktonic foraminifera, *Paleoceanography*, *25*, PA2215, doi:10.1029/2009PA001796.

Broecker, W. S., and E. Clark (2001), Glacial-to-Holocene redistribution of carbonate ion in the deep sea, *Science*, *294*(5549), 2152–2155, doi:10.1126/science.1064171.

Brown, S. J., and H. Elderfield (1996), Variations in Mg/Ca and Sr/Ca ratios of planktonic foraminifera caused by postdepositional dissolution: Evidence of shallow Mg-dependent dissolution, *Paleoceanography*, *11*(5), 543–551.

Chen, J.-M., C.-P. Chang, and T. Li (2003), Annual cycle of the South China sea surface temperature using the NCEP/NCAR reanalysis, *J. Meteorol. Soc. Jpn.*, *81*(4), 879–884, doi:10.2151/jmsj.81.879.

Chou, W.-C., D. D. Sheu, B. S. Lee, C. M. Tseng, C. T. A. Chen, S. L. Wang, and G. T. F. Wong (2007), Depth distributions of alkalinity, TCO_2 and $\delta^{13}C_{TCO2}$ at SEATS time-series site in the northern South China Sea, *Deep-Sea Res. II*, *54*, 1469–1485, doi:10.1016/j.dsr2.2007.05.002.

Chu, P. C., and W. Guihua (2003), Seasonal variability of thermohaline front in the Central South China sea, *J. Oceanogr.*, *59*(1), 65–78, doi:10.1023/A:1022868407012.

Conan, S. M.-H., E. M. Ivanova, and G.-J. A. Brummer (2002), Quantifying carbonate dissolution and calibration of foraminiferal dissolution indices in the Somali Basin, *Mar. Geol.*, *182*(3-4), 325–349, doi:10.1016/S0025-3227(01)00238-9.

de Villiers, S. (2005), Foraminiferal shell-weight evidence for sedimentary calcite dissolution above the lysocline, *Deep-Sea Res. I*, *52*(5), 671–680, doi:10.1016/j.dsr.2004.11.014.

Dekens, P. S., D. W. Lea, D. K. Pak, and H. J. Spero (2002), Core top calibration of Mg/Ca in tropical foraminifera: Refining paleotemperature estimation, *Geochem. Geophys. Geosyst.*, *3*(4), 1–29, doi:10.1029/2001GC000200.

Dickson, A. G. (1990), Standard potential of the reaction: Ag(Cl)(s) + 1/2 H_2(g) = Ag(s) + HCl(aq), and the standard acidity constant ot the ion HSO_4^- in synthetic seawater from 273.15 to 318.15 K, *J. Chem. Thermodyn.*, *22*(2), 113–127, doi:10.1016/0021-9614(90)90074-Z.

Dickson, A. G., and F. J. Millero (1987), A comparison of the equilibrium constants for the dissociation of carbonic acid in seawater media, *Deep-Sea Res.*, *34*, 1733–1743, doi:10.1016/0198-0149(87)90021-5.

Dunn, D. A., T. C. Moore Jr., and L. D. Keigwin Jr. (1981), Atlantic-type carbonate stratigraphy in the late Miocene Pacific, *Nature*, *291*, 225–227, doi:10.1038/291225a0.

Dunne, J. P., J. R. Toggweiler, and B. Hales (2012), Global calcite cycling constrained by sediment preservation controls, *Global Biogeochem. Cycles*, *26*, GB3023, doi:10.1029/2010GB003935.

Duplessy, J.-C., P.-L. Blanc, and A. W. H. Bé (1981), Oxygen-18 enrichment of planktic foraminifera due to gametogenic calcification below the euphotic zone, *Science*, *213*(4513), 1247–1250, doi:10.1126/science.213.4513.1247.

Elderfield, H., and G. Ganssen (2000), Past temperature and δ^{18}O of surface ocean waters inferred from foraminiferal Mg/Ca ratios, *Nature*, *405*, 442–445, doi:10.1038/35013033.

Elderfield, H., M. Vautravers, and M. Cooper (2002), The relationship between shell size and Mg/Ca, Sr/Ca, δ^{18}O, and δ^{13}C of species of planktonic foraminifera, *Geochem. Geophys. Geosyst.*, *3*(8), 1–13, doi:10.1029/2001GC000194.

Fairbanks, R. G., M. Sverdlove, R. Free, P. H. Wiebe, and A. W. H. Bé (1982), Vertical distribution and isotopic fractionation of living planktonic foraminifera from the Panama Basin, *Nature*, *298*, 841–844, doi:10.1038/298841a0.

Fallet, U., I. S. Castañeda, A. Henry-Edwards, T. O. Richter, W. Boer, S. Schouten, and G.-J. Brummer (2012), Sedimentation and burial of organic and inorganic temperature proxies in the Mozambique Channel, SW Indian Ocean, *Deep-Sea Res. I*, *59*, 37–53, doi:10.1016/j.dsr.2011.10.002.

Farmer, E. C., A. Kaplan, P. B. deMenocal, and J. Lynch-Stieglitz (2007), Corroborating ecological depth preferences of planktonic foraminifera in the tropical Atlantic with the stable oxygen isotope ratios of core top specimens, *Paleoceanography*, *22*(3), PA3205, doi:10.1029/2006PA001361.

Farrell, J. F., and W. L. Prell (1989), Climatic change and $CaCO_3$ preservation: An 800,000 year bathymetric reconstruction from the central equatorial Pacific Ocean, *Paleoceanography*, *4*(4), 447–466, doi:10.1029/PA004i004p00447.

Feely, R. A., C. L. Sabine, K. Lee, W. Berelson, J. Kleypas, V. J. Fabry, and F. J. Millero (2004), Impact of anthropogenic CO_2 on the $CaCO_3$ system in the oceans, *Science*, *305*, 362–366, doi:10.1126/science.1097329.

Fehrenbacher, J., and P. A. Martin (2011), Western equatorial Pacific deep water carbonate chemistry during the Last Glacial Maximum and deglaciation: Using planktic foraminiferal Mg/Ca to reconstruct sea surface temperature and seafloor dissolution, *Paleoceanography*, *26*, PA2225, doi:10.1029/2010PA002035.

Fehrenbacher, J., P. A. Martin, and G. Eshel (2006), Glacial deep water carbonate chemistry inferred from foraminiferal Mg/Ca: A case study from the western tropical Atlantic, *Geochem. Geophys. Geosyst.*, *7*, Q09P16, doi:10.1029/2005GC001156.

Friedrich, O., R. Schiebel, P. A. Wilson, S. Weldeab, C. J. Beer, M. J. Cooper, and J. Fiebig (2012), Influence of test size, water depth, and ecology on Mg/Ca, Sr/Ca, δ^{18}O and δ^{13}C in nine modern species of planktic foraminifers, *Earth. Planet. Sci. Lett.*, *319-320*, 133–145, doi:10.1016/j.epsl.2011.12.002.

Greaves, M., et al. (2008), Interlaboratory comparison study of calibration standards for foraminiferal Mg/Ca thermometry, *Geochem. Geophys. Geosyst.*, *9*, Q08010, doi:10.1029/2008GC001974.

Haijun, Y., L. Qinyu, and J. Xujing (1999), On the upper oceanic heat budget in the South China Sea: Annual cycle, *Adv. Atmos. Sci.*, *16*(4), 619–629, doi:10.1007/s00376-999-0036-x.

Hertzberg, J. E., and M. W. Schmidt (2013), Refining Globigerinoides ruber Mg/Ca paleothermometry in the Atlantic Ocean, *Earth. Planet. Sci. Lett.*, *383*, 123–133, doi:10.1016/j.epsl.2013.09.044.

Holbourn, A. E., W. Kuhnt, M. Regenberg, M. Schulz, A. Mix, and N. Andersen (2010), Does Antarctic glaciation force migration of the tropical rain belt?, *Geology*, *38*, 783–786, doi:10.1130/G31043.1.

Jansen, H., R. E. Zeebe, and D. A. Wolf-Gladrow (2002), Modeling the dissolution of settling $CaCO_3$ in the ocean, *Global Biogeochem. Cycles*, *16*(2), 1027, doi:10.1029/2000GB001279.

Johnstone, H. J. H., J. Yu, H. Elderfield, and M. Schulz (2011), Improving temperature estimates derived from Mg/Ca of planktonic foraminifera using X-ray computed tomography-based dissolution index, XDX, *Paleoceanography*, *26*, PA1215, doi:10.1029/2009PA001902.

Keenlyside, N. S., M. Latif, and A. Dürkop (2007), On sub-ENSO variability, *J. Clim.*, *20*, 3452–3469, doi:10.1175/JCLI4199.1.

Koutavas, A., J. Lynch-Stieglitz, T. M. Marchitto Jr., and J. Sachs (2002), El Niño-like pattern in Ice Age tropical pacific sea surface temperature, *Science*, *297*(5579), 226–230, doi:10.1126/science.1072376.

Lea, D. W., T. A. Mashiotta, and H. J. Spero (1999), Controls on the magnesium and strontium uptake in planktonic foraminifera determined by live culturing, *Geochim. Cosmochim. Acta*, *63*(16), 2369–2379, doi:10.1016/S0016-7037(99)00197-0.

Lea, D. W., D. K. Pak, and H. J. Spero (2000), Climate impact of late quaternary equatorial Pacific sea surface temperature variations, *Science*, *289*(5485), 1719–1724, doi:10.1126/science.289.5485.1719.

Lea, D. W., D. K. Pak, and G. Paradis (2005), Influence of volcanic shards on foraminiferal Mg/Ca in a core from the Galápagos region, *Geochem. Geophys. Geosyst.*, *6*, Q11P04, doi:10.1029/2005GC000970.

LeGrande, A. N., J. Lynch-Stieglitz, and E. C. Farmer (2004), Oxygen isotopic composition of *Globorotalia truncatulinoides* as a proxy for intermediate depth intensity, *Paleoceanography*, *19*, PA4025, doi:10.1029/2004PA001045.

Lewis, E., and D. W. R. Wallace (eds.) (1998), *CO2SYS–Program Developed for CO_2 System Calculations. ORNL/CDIAC-105*, Carbon Dioxide Information Analysis Center, Oak Ridge National Laboratory, U.S. Department of Energy, Oak Ridge, Tennessee.

Lončarić, N., F. J. C. Peeters, D. Kroon, and G.-J. A. Brummer (2006), Oxygen isotope ecology of recent planktic foraminifera at the central Walvis Ridge (SE Atlantic), *Paleoceanography*, *21*, PA3009, doi:10.1029/2005PA001207.

Lorens, R. B., D. F. Williams, and M. L. Bender (1977), The early nonstructual chemical diagenesis of foraminiferal calcite, *J. Sediment. Res.*, *47*(4), 1602–1609, doi:10.1306/212F73C9-2B24-11D7-8648000102C1865D.

Martin, P. A., and D. W. Lea (2002), A simple evaluation of cleaning procedures on fossil benthic foraminiferal Mg/Ca, *Geochem. Geophys. Geosyst.*, *3*(10), 8401, doi:10.1029/2001GC000280.

Martin, W. R., and F. L. Sayles (2003), The recycling of biogenic material at the seafloor, in *Treatise on Geochemistry - The Oceans and Marine Geochemistry,* vol. 7, edited by F. T. Mackenzie, pp. 37–66, Elsevier Ltd., Oxford.

McKenna, V. S., and W. L. Prell (2004), Calibration of the Mg/Ca of *Globorotalia truncatulinoides* (R) for the reconstruction of marine temperature gradients, *Paleoceanography*, *19*, PA2006, doi:10.1029/2000PA000604.
Mehrbach, C., C. H. Culberson, J. E. Hawley, and R. M. Pytkowicz (1973), Measurement of the apparent dissociation constants of carbonic acid in seawater at atmospheric pressure, *Limnol. Oceanogr.*, *18*, 897–907.
Mekik, F., and R. François (2006), Tracing deep-sea calcite dissolution: Agreement between the *Globorotalia menardii* fragmentation index and elemental ratios (Mg/Ca and Mg/Sr) in planktonic foraminifers, *Paleoceanography*, *21*, PA4219, doi:10.1029/2006PA001296.
Mulitza, S., A. Dürkoop, W. Hale, and G. Wefer (1997), Planktonic foraminifera as recorders of past surface-water stratification, *Geology*, *25*(4), 335–338.
NODC (2001), National Oceanographic and Data Center, World Ocean Atlas 2001: Objective Analyses, Data Statistics, and Figures, *CD-ROM Documentation*, Natl. Oceanic and Atmos. Admin., Silver Spring, Md., http://www.nodc.noaa.gov/.
Pahnke, K., R. Zahn, H. Elderfield, and M. Schulz (2003), 340,000-Year centennial-scale marine record of southern hemisphere climatic oscillation, *Science*, *301*(5635), 948–952, doi:10.1126/science.1084451.
Regenberg, M., D. Nürnberg, S. Steph, J. Groeneveld, D. Garbe-Schönberg, R. Tiedemann, and W.-C. Dullo (2006), Assessing the dissolution effect on planktonic foraminiferal Mg/Ca ratios: Evidence from Caribbean core-tops, *Geochem. Geophys. Geosyst.*, *7*, Q07P15, doi:10.1029/2005GC001019.
Regenberg, M., D. Nürnberg, J. Schönfeld, and G.-J. Reichart (2007), Early diagenetic overprint in Caribbean sediment cores and its effect on the geochemical composition of planktonic foraminifera, *Biogeosciences*, *4*, 957–973, doi:10.5194/bg-4-957-2007.
Regenberg, M., S. Steph, D. Nürnberg, R. Tiedemann, and D. Garbe-Schönberg (2009), Calibrating Mg/Ca ratios of multiple planktonic foraminiferal species with δ^{18}O-calcification temperatures: Paleothermometry for the upper water column, *Earth. Planet. Sci. Lett.*, *278*, 324–336, doi:10.1016/j.epsl.2008.12.019.
Regenberg, M., S. N. Nielsen, W. Kuhnt, A. Holbourn, D. Garbe-Schönberg, and N. Andersen (2010), Morphological, geochemical, and ecological differences of the extant menardiform planktonic foraminifera Globorotalia menardii and Globorotalia cultrata, *Mar. Micropaleontol.*, *74*, 96–107, doi:10.1016/j.marmicro.2010.01.002.
Rosenthal, Y., and E. A. Boyle (1993), Factors controlling the flouride content of planktonic foraminifera: An evaluation of its paleoceanographic applicability, *Geochim. Cosmochim. Acta*, *57*(2), 335–346, doi:10.1016/0016-7037(93)90435-Y.
Rosenthal, Y., and B. Linsley (2007), Mg/Ca and Sr/Ca paleothermometery from calcareous marine fossils, in *Encyclopedia of Quaternary Sciences*, edited by S. A. Elias, pp. 1723–1731, Elsevier, London.
Rosenthal, Y., and G. P. Lohmann (2002), Accurate estimation of sea surface temperatures using dissolution-corrected calibrations for Mg/Ca paleothermometry, *Paleoceanography*, *17*(3), 1044, doi:10.1029/2001PA000749.
Rosenthal, Y., et al. (2004), Interlaboratory comparison study of Mg/Ca and Sr/Ca measurements in planktonic foraminifera for paleoceanographic research, *Geochem. Geophys. Geosyst.*, *5*, Q04D09, doi:10.1029/2003GC000650.
Russell, A. D., S. Emerson, B. K. Nelson, J. Erez, and D. W. Lea (1994), Uranium in foraminiferal calcite as a recorder of seawater uranium concentrations, *Geochim. Cosmochim. Acta*, *58*(2), 671–681, doi:10.1016/0016-7037(94)90497-9.
Sadekov, A. Y., S. M. Eggins, G. Klinkhammer, and Y. Rosenthal (2010), Effects of seafloor and laboratory dissolution on the Mg/Ca composition of Globigerinoides sacculifer and Orbulina universa tests – A laser ablation ICPMS microanalysis perspective, *Earth. Planet. Sci. Lett.*, *292*, 312–324, doi:10.1016/j.epsl.2010.01.039.
Sarnthein, M., U. Pflaumann, P. X. Wang, and H. K. Wong (eds.) (1994), *Preliminary Report on SONNE-95 Cruise "Monitor Monsoon" to the South China Sea*, Geol.-Paläontol. Inst. Universität Kiel, Kiel, Germany.
Schiebel, R., and C. Hemleben (2005), Modern planktic foraminifera, *Paläontol. Z.*, *79*, 135–148, doi:10.1007/BF03021758.
Schmidt, M. W., M. J. Vautravers, and H. J. Spero (2006), Rapid subtropical North Atlantic salinity oscillations across Dansgaard-Oeschger cycles, *Nature*, *443*, 561–564, doi:10.1038/nature05121.
Stattegger, K., W. Kuhnt, H. K. Wong, and Scientific Party (1997), *Cruise Report SONNE 115 SUNDAFLUT*, Geol.-Paläontol. Inst. Universität Kiel, Kiel, Germany.
Steinke, S., H.-Y. Chiu, P.-S. Yu, C.-C. Shen, L. Löwenmark, H.-S. Mii, and M.-T. Chen (2005), Mg/Ca ratios of two Globigerinoides ruber (white) morphotypes: Implications for reconstructing past tropical/subtropical surface water conditions, *Geochem. Geophys. Geosyst.*, *6*, Q11005, doi:10.1029/2005GC000926.
Steph, S., M. Regenberg, R. Tiedemann, S. Mulitza, and D. Nürnberg (2009), Stable isotopes of planktonic foraminifera from tropical Atlantic/Caribbean core-tops: Implications for reconstructing upper ocean stratification, *Mar. Micropaleontol.*, *71*, 1–19, doi:10.1016/j.marmicro.2008.12.004.
Tseng, C.-M., G.-C. Gong, L.-W. Wang, K.-K. Liu, and Y. Yang (2009a), Anomalous biogeochemical conditions in the northern South China Sea during the El-Niño events between 1997 and 2003, *Geophys. Res. Lett.*, *36*, L14611, doi:10.1029/2009GL038252.
Tseng, C.-M., K.-K. Liu, L.-W. Wang, and G.-C. Gong (2009b), Anomalous hydrographic and biological conditions in the northern South China Sea during the 1997–1998 El Niño and comparisons with the equatorial Pacific, *Deep-Sea Res. I*, *56*, 2129–2143, doi:10.1016/j.dsr.2009.09.004.
Vautard, R., and M. Ghil (1989), Singular spectrum analysis in nonlinear dynamics, with application to paleoclimatic time series, *Physica D*, *35*(3), 395–424, doi:10.1016/0167-2789(89)90077-8.
Wang, P., and Q. Li (2009), Oceanographical and geological background, in *The South China Sea, Development in Paleoenvironmental Research,* vol. 13, edited by P. Wang and Q. Li, pp. 25–73, Springer Science+Business Media B.V., Netherlands, doi:10.1007/978-1-4020-9745-4-2.
Wang, W., and C. Wang (2006), Formation and decay of the spring warm pool in the South China Sea, *Geophys. Res. Lett.*, *33*, L02615, doi:10.1029/2005GL025097.
Whitko, A. N., D. W. Hastings, and B. P. Flower (2002), Past sea surface temperatures in the tropical South China Sea based on a new foraminiferal Mg calibration, *MARSci*, MARSci.2002.01.020101.
Wiesner, M. G., K. Stattegger, and W. Kuhnt (eds.) (1999), *Cruise Report SONNE 140 SÜDMEER III*, Inst. für Geowiss. Universität Kiel, Kiel, Germany.
Xu, J., W. Kuhnt, A. Holbourn, M. Regenberg, and N. Andersen (2010), Indo-Pacific warm pool variability during the Holocene and Last Glacial Maximum, *Paleoceanography*, *25*, PA4230, doi:10.1029/2010PA001934.
Zhou, F., and R. Gao (2003), Intraseasonal variability of the subsurface temperature observed in the South China Sea (SCS), *Chinese Sci. Bull.*, *47*(4), 337–342, doi:10.1360/02tb9081.
Ziegler, M., D. Nürnberg, C. Karas, R. Tiedemann, and L. J. Lourens (2008), Persistent summer expansion of the Atlantic Warm Pool during glacial abrupt cold events, *Nat. Geosci.*, *1*, 601–605, doi:10.1038/ngeo277.